

# Background reduction and sensitivity for germanium double beta decay experiments

H. Gómez<sup>\*</sup>, S. Cebrián, J. Morales, J.A. Villar

*Laboratorio de Física Nuclear y Altas Energías, Universidad de Zaragoza, 50009 Zaragoza, Spain*

---

## Abstract

Germanium detectors have very good capabilities for the investigation of rare phenomena like the neutrinoless double beta decay. Rejection of the background entangling the expected signal is one primary goal in this kind of experiments. Here, the attainable background reduction in the energy region where the neutrinoless double beta decay signal of  $^{76}\text{Ge}$  is expected to appear has been evaluated for experiments using germanium detectors, taking into consideration different strategies like the granularity of the detector system, the segmentation of each individual germanium detector and the application of Pulse Shape Analysis techniques to discriminate signal from background events. Detection efficiency to the signal is affected by background rejection techniques, and therefore it has been estimated for each of the background rejection scenarios considered. Finally, conditions regarding crystal mass, radiopurity, exposure to cosmic rays, shielding and rejection capabilities are discussed with the aim to achieve a background level of  $\sim 10^{-3} \text{ c keV}^{-1} \text{ kg}^{-1} \text{ y}^{-1}$  in the region of interest, which would allow to explore neutrino effective masses around  $\sim 40 \text{ meV}$ .

*Key words:* double beta decay, germanium detectors, granularity, segmentation, pulse shape analysis, sensitivity

*PACS:* 14.60.Pq, 23.40.-s, 24.10.Lx, 29.40.-n

---

## 1. Introduction

Investigation of neutrinoless Double Beta Decay (DBD) can shed light on interesting pending questions like the absolute values of the neutrino mass and the properties of neutrinos under CP-conjugation [1]. Germanium detectors enriched in double beta decay emitter  $^{76}\text{Ge}$ , offer important advantages for this investigation in comparison with other kind of detectors and nuclei [2,3]: excellent energy resolution, high purity materials and powerful background rejection capabilities, well established detector technologies, favorable nuclear matrix element, high transition energy  $Q$  around 2039 keV [4], . . . . Indeed, germanium double beta decay experiments (Heidelberg-Moscow and IGEX) have provided the most restrictive bounds on the effective neutrinos mass [5,6].

Both Heidelberg-Moscow and IGEX experiments, presently finished, followed similar strategies using several massive high-purity germanium detectors (HPGe) (around 2 kg each) with close-end coaxial geometries together

with active and passive shieldings in deep underground laboratories. As a continuation of these experiments, next-generation projects as Majorana [7] and GERDA [8], have been proposed incorporating different innovations like using segmented germanium detectors or operating naked crystals in cryogenic liquids, like nitrogen or argon.

Important advances in high-purity germanium detector technologies have been achieved in the last years [9], allowing the construction of large efficiency HPGe crystals and developing the monolithic segmentation technique which provides both interaction position and energy information. The analysis of pulse shapes in highly segmented germanium detectors (taking into account not only net signals in a segment but also induced transient signals in the neighboring segments) has revealed as a promising technique for three-dimensional position determination [10]. First results of the operation of segmented germanium crystals within DBD projects have recently been presented [11,12]. Important achievements have been obtained in other contexts for the spatial resolution of events (see for instance Refs. [13]-[16]), greatly surpassing the position determination capabilities of previous DBD germanium experiments based on pulse shape discrimination in conventional germanium detectors [17]. The main difference between real double beta

---

<sup>\*</sup> Corresponding Author: Laboratorio de Física Nuclear y Altas Energías, Facultad de Ciencias, Pedro Cerbuna 12, 50009 Zaragoza, Spain. Phone number: 34 976761246. Fax number: 34 976761247  
*Email address:* hgomez@unizar.es (H. Gómez).

decay and background events is that the former leave generally only one energy deposit inside the crystal ("monosite" events), whereas the latter leave in many cases more than one ("multisite" events). For this reason, thanks to the analysis of pulse shapes, only background events producing one energy deposit in the crystal can be mistaken with real double beta decay events. One goal of this work is therefore to evaluate the background reduction attainable at present for germanium detectors in the region between 2 and 2.1 MeV where the neutrinoless double beta decay signal of  $^{76}\text{Ge}$  is expected to appear. Reduction of background is based on the granularity of the detector system, on the segmentation of each individual germanium detector and on the application of Pulse Shape Analysis (PSA) techniques to discriminate signal from background events.

In underground experiments searching for rare events like the nuclear double beta decay, the background entangling the expected signal comes mainly from environmental gamma radiations (including radon emissions) and neutrons at the laboratory, radioactive impurities (either primordial or cosmogenically induced) in the materials of the experimental set-up and cosmic muons arriving even deep underground [18,19]. To explore effective neutrino masses around 40 meV, a background level  $\sim 10^{-3}$  c keV $^{-1}$  kg $^{-1}$  y $^{-1}$  in the region of interest must be achieved in germanium double beta decay experiments. The two main sources of the background registered in the region of interest for the neutrinoless double beta decay of  $^{76}\text{Ge}$  have been identified in previous experiments like IGEX to be cosmogenic activation of germanium detectors (mainly  $^{68}\text{Ge}$  and  $^{60}\text{Co}$ ) [20] and external gamma background above 2 MeV coming from  $^{232}\text{Th}$  and  $^{238}\text{U}$  chains. In fact, in present projects of new experiments these two sources continue to be a dominant background [7,8]. Therefore, in this work the particular background components thought to be the most significant ones will be taken into account: cosmogenic  $^{68}\text{Ge}$  and  $^{60}\text{Co}$  produced in the germanium crystal and the 2614.5 keV emission from  $^{208}\text{Tl}$  in the  $^{232}\text{Th}$  chain. Precise conditions necessary to achieve a background level  $\sim 10^{-3}$  c keV $^{-1}$  kg $^{-1}$  y $^{-1}$  in the region of interest from these sources will be discussed. Recently, a Monte Carlo study of the background achievable in the GERDA experiment by anti-coincidence cuts between crystals and segments has been published considering the main radioactive impurities in the set-up [21]; it has also been shown in the context of this experiment that muon-induced contribution to background can be of  $\sim 10^{-4}$  c keV $^{-1}$  kg $^{-1}$  y $^{-1}$  provided that muon veto system is used [22].

The paper is organized in the following way. In Sec. 2 the raw backgrounds expected from the relevant sources are studied, including results from a recent evaluation of the production rates of the most relevant cosmogenic products in germanium detectors at sea level. Then, the analysis of the effects of each one of the three reduction strategies considered (granularity, segmentation and PSA) for the different background sources will be presented in Sec. 3. Detection efficiency to the neutrinoless DBD signal and

corresponding sensitivity will be studied in Sec. 4 assuming the different background rejection scenarios. Finally, results and conclusions will be discussed in Sec. 5.

## 2. Raw backgrounds

An attempt has been made to estimate the raw contributions to the detector counting rates coming from the main sources of background taken into account, before applying any technique for background reduction.

For this estimate, and for the study of the different background reduction strategies presented in the next section, a set of Monte Carlo simulations using GEANT4 [23] package has been developed. As the first goal was focused on the crystal geometry, a natural germanium crystal without shielding has been defined as detector. Internal contaminations of the crystal are emitted homogeneously inside it, whereas for external sources, the corresponding gammas were emitted homogeneously and isotropically from the surface of an external sphere. Standard GEANT4 models, including those specific for low energy, have been used for all the processes, isotopes decays, and particles simulated. For every simulation made, position and energy of each interaction produced in an event have been registered. This information has allowed us to make different analysis of the obtained data in the Region of Interest (RoI) between 2 and 2.1 MeV. It has been simulated a number of events big enough to obtain a negligible statistical error (below 2% for all the studies made).

### 2.1. Cosmogenic radioactivity

Long-lived radioactive nuclei induced by the exposure of the materials of the set-up to cosmic rays at sea level (during fabrication, transport and storage) may become very problematic for rare event experiments which operate in deep underground locations, using active and passive shields and selecting carefully radiopure components. Therefore, materials must be kept shielded against the hadronic component of the cosmic rays to prevent cosmogenic activation, flying must be avoided and the exposure on the surface of the Earth should be reduced as much as possible. Since these requirements usually complicate the preparation of experiments (for example, crystal growth and mounting of detectors) it would be desirable to have reliable tools to quantify the real danger of exposing the materials to cosmic rays.

For these reasons, cosmogenic activation in germanium double beta decay experiments was specifically studied in Ref. [24]. Using these and previous results from the literature, together with specific simulations of the response to the cosmogenic background of germanium detectors, the expected counting rate due to this effect in the neutrinoless DBD region has been evaluated.

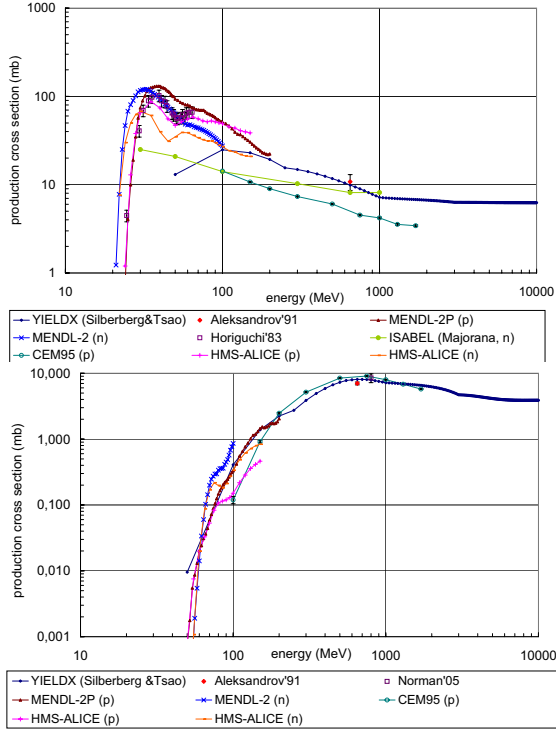


Fig. 1. Comparison of excitation functions for  $^{68}\text{Ge}$  (top) and for  $^{60}\text{Co}$  (bottom) in natural germanium by nucleons from different sources: measurements (Horiguchi'83 [25], Aleksandrov'91 [26] and Norman'05 [27]), calculations using the YIELDX code [28], and Monte Carlos results (elaborated by the Majorana Collaboration using ISABEL [7], taken from the MENDL2 libraries based on ALICE code [29] and taken from the library in Refs. [30,31] using CEM95 and HMS-ALICE codes).

### 2.1.1. Production rates

Excitation functions of  $^{60}\text{Co}$  and  $^{68}\text{Ge}$ , as well as of other long-lived products induced in germanium, have been compiled using available measurements and different calculations taken from libraries or made on purpose in Ref. [24] (see Figure 1). In an attempt to find the most reliable selection of the excitation functions, those calculations with minimum deviations with respect to experimental data were taken into consideration: below 150 MeV, HMS-ALICE results for neutrons [30,31], and above this energy, YIELDX calculations.

Once chosen the excitation functions, production rates of  $^{60}\text{Co}$  and  $^{68}\text{Ge}$  were calculated using the cosmic neutron spectrum from Ziegler [32], for both natural and enriched germanium (86% of  $^{76}\text{Ge}$ , 14% of  $^{74}\text{Ge}$ ). Results are summarized in Tables 1 and 2, compared with some previous estimates.

A production rate of  $\sim 5 \text{ kg}^{-1}\text{d}^{-1}$  can be safely considered in natural Ge for  $^{60}\text{Co}$  while for  $^{68}\text{Ge}$  the production rate of  $\sim 90 \text{ kg}^{-1}\text{d}^{-1}$  found in this work is significantly higher than in previous estimates including the measurements in Ref. [35] due to the large contribution of neutrons below 100 MeV. Since there is now no available measurement of production cross sections by neutrons for the relevant isotopes, it is difficult to assess to what extent the two basic assumptions of the presented calculations are valid.

For enriched detectors, production of  $^{68}\text{Ge}$ , although much more reduced than the one for natural germanium, has been found one order of magnitude higher than previous estimates commonly used [34,35].  $^{60}\text{Co}$  production seems to be similar in enriched and natural material.

### 2.1.2. Counting rates in the region of interest

A set of Monte Carlo simulations based on GEANT4 code have been made to reproduce the response of cylindrical germanium detectors of different masses to the background sources, including  $^{60}\text{Co}$  and  $^{68}\text{Ge}$  isotopes induced in the germanium crystal.

The number of events registered in the 2-2.1 MeV RoI per isotope decay can be deduced using these MC simulations. For 2(4)-kg detectors, these numbers are 0.00016 (0.00020) c/keV/decay of  $^{60}\text{Co}$  and 0.00023 (0.00029) c/keV/decay of  $^{68}\text{Ge}$  (in agreement with the ones deduced in simulations made by the Majorana [7] and GERDA [8] collaborations).

Using this information from GEANT4 simulations together with the production rates previously presented, the counting rates in the region of interest due to the cosmogenic contaminations can be derived for certain exposure and cooling times of the material. To properly compare results, the same times typically used in the GERDA project [36] will be considered: 30 days of exposure to cosmic rays for  $^{60}\text{Co}$  production and 180 days of exposure plus 180 days of cooling for  $^{68}\text{Ge}$ . Table 3 presents the obtained counting rates in these conditions and using production rates of  $5 \text{ kg}^{-1}\text{d}^{-1}$  for  $^{60}\text{Co}$  and  $1 \text{ kg}^{-1}\text{d}^{-1}$  for  $^{68}\text{Ge}$ ; it is also shown the estimate when considering a  $^{68}\text{Ge}$  production rate of  $10 \text{ kg}^{-1}\text{d}^{-1}$  and 2 years of cooling. As it can be seen, for this high  $^{68}\text{Ge}$  production rate it would be necessary to wait more than two years (instead of 3 months) to achieve counting rates of the same order than when considering the low production rate. Rates presented in Table 3 correspond to conventional germanium detectors, that is, without taking into account neither segmentation nor PSA techniques.

## 2.2. 2614.5 keV $^{208}\text{Tl}$ emissions

An evaluation of the expected background coming from the 2614.5 keV line from  $^{208}\text{Tl}$  has been made, considering both the environmental gamma background in the laboratory and the  $^{232}\text{Th}$  intrinsic radioimpurities in the lead shielding expected to be surrounding detectors. The response to 2614.5 keV photons for the counting rates in the 2-2.1 MeV RoI in 2-kg and 4-kg germanium detectors has been estimated by Monte Carlo simulation. A flux of  $\sim 0.1 \text{ cm}^{-2} \text{ s}^{-1}$  for environmental 2614.5 keV photons has been assumed, according to recent measurements in the new Canfranc Underground Laboratory [37], and an activity of  $1 \mu\text{Bq/kg}$  of  $^{232}\text{Th}$  in lead has been considered just as a reference value. In these estimates, a spherical cavity with radius  $R=30 \text{ cm}$  for placing detectors inside has been supposed, and two different shielding configurations with 30

Table 1

Production rates (in  $\text{kg}^{-1}\text{d}^{-1}$ ) in natural germanium obtained considering HMS-ALICE and YIELDX below and above 150 MeV respectively, together with previous estimates. Some results from Ref. [35] are based on Monte Carlo calculations (MC) while others come from measurements (exp).

	HMS-ALICE+YIELDX [24]	Ref. [33]	Ref. [34]	Ref. [35] (MC)	Ref. [35] (exp)
$^{68}\text{Ge}$	77+12=89	58.4	26.5	29.6	30±7
$^{60}\text{Co}$	0.3+4.5=4.8	6.6	4.8		

Table 2

As Table 1, but for enriched germanium (86% of  $^{76}\text{Ge}$  and 14% of  $^{74}\text{Ge}$ ).

	HMS-ALICE+YIELDX [24]	Ref. [34]	Ref. [35]
$^{68}\text{Ge}$	2.8+10=13	1.2	0.94
$^{60}\text{Co}$	0.02+6.7=6.7	3.5	

Table 3

Estimates of counting rates R (in units of  $10^{-3} \text{ c keV}^{-1} \text{ kg}^{-1}\text{y}^{-1}$ ) in the 2-2.1 MeV RoI from cosmogenic contaminations in 2-kg and 4-kg germanium detectors. Uncertainties in these estimates are discussed in the text.

	production rate	exposure	cooling	R	R
	( $\text{kg}^{-1}\text{d}^{-1}$ )	(d)	(d)	2 kg	4 kg
$^{60}\text{Co}$	5	30	0	2.9	3.7
$^{68}\text{Ge}$	1	180	180	12	16
$^{68}\text{Ge}$	10	180	730	31	39

Table 4

Estimates of counting rates (in units of  $10^{-3} \text{ c keV}^{-1} \text{ kg}^{-1}\text{y}^{-1}$ ) in the 2-2.1 MeV RoI from 2614.5 keV  $^{208}\text{Tl}$  emissions in 2-kg and 4-kg germanium detectors (see text). Two shielding configurations with 30 and 40 cm of lead have been taken into consideration. Uncertainties in these estimates are discussed in the text.

	2 kg	4 kg
external gamma, 30 cm Pb	40	32
external gamma, 40 cm Pb	0.38	0.30
intrinsic radioimpurities in Pb	2.8	2.2

and 40 cm of lead surrounding the cavity have been taken into account. Table 4 summarizes the obtained results.

For the intrinsic radioimpurities in the lead shielding, it has been checked that around 90% of the events come from the most internal 5 cm of shield, and in fact, virtually the same counting rates have been found when considering 30 or 40 cm of lead (despite the significant difference in mass and consequently in  $^{232}\text{Th}$  activity between the two configurations). For the external gamma background, the additional 10 cm when assuming a 40-cm-thick lead layer reduce the counting rates around two orders of magnitude. Comparing the background levels expected in 2 and 4-kg detectors in Tables 3 and 4, the largest crystals have a lower background level ( $\sim 20\%$ ) from  $^{208}\text{Tl}$  but higher counting rates ( $\sim 30\%$ ) from internal cosmogenic impurities. This fact will be discussed at Sec. 3.1.

Uncertainties in the estimates of raw backgrounds presented in Tables 3 and 4 come in principle from the simulations of the response of detectors to the different background sources as well as from the inputs considered for production rates of cosmogenic isotopes and levels of  $^{208}\text{Tl}$  photons. Counting rates are directly proportional to these inputs, which are thought to be the main source of error since GEANT4 can reproduce electromagnetic processes

with a few per cent error and statistical errors in simulations have always been kept below 2% as stated before. Production rate of  $^{60}\text{Co}$  has an uncertainty of  $\sim 50\%$  (when considering different available estimates) and for  $^{68}\text{Ge}$  it could be up to one order of magnitude. Environmental gamma fluxes depend on the particular underground location. For  $^{232}\text{Th}$  impurities in very pure lead just upper bounds have been derived (see Refs. [38,39]) and therefore the assumed value must be taken just as a reference.

### 3. Rejection of background events

The main goal in the study of the different ways to reduce the background was to try to analyze the correlation between the experiment design and background level in the region of interest. Assuming a hypothetical final set up of an experiment with a total mass of germanium around some tens of kilograms, the aim was to determine what is the optimal mass distribution and features of detectors to have a background level as low as possible. Three topics that can determine the best configuration, as we pointed out before, are: granularity of the experiment detectors, segmentation of the crystals and analysis of the obtained pulses.

### 3.1. Granularity

The first step to determine the best set up of the experiment consists in analyzing what could be the optimal mass of the detectors that build the whole experiment to have a background level as low as possible, if a fixed total mass of germanium is assumed. With this purpose, cylindrical crystals with the same value for diameter and height and masses between 0.1 and 4 kg have been simulated.

If only the events with an energy deposit between 2 and 2.1 MeV are taken into account, we can see how for internal contaminations and a given specific activity, the higher mass detectors register a higher background level (see Figs.2 a,b). 4-kg detectors register 28% (26%) more events for  $^{60}\text{Co}$  ( $^{68}\text{Ge}$ ) than 2-kg ones. This is not the case for external contaminations, because for a given activity, the heavier detectors have a lower background (see Fig.2 c). 4-kg detectors register 54% less events coming from 2614.5 keV photons than 2-kg detectors. These values confirm that the optimal configuration of an experiment depends on what kind of background we want to reduce more, that coming from internal contaminations or from external ones, taking also into account that the dependency between the mass of the detectors and the background events registered is stronger for the external contamination. These data together with conclusions obtained from the study of the segmentation of the crystal and pulse analysis, as explained later, will determine the best configuration.

### 3.2. Segmentation

Regardless of the mass of the used detectors, other way to reduce the background level is by segmentation of the crystals and further application of anticoincidence techniques between segments. The aim was to quantify the maximum background reduction that could be obtained from segmentation of the crystals. For the cylindrical detectors studied, two different ways to divide it were considered: segmentation in planes and segmentation in sectors (longitudinal and transversal segmentation respectively) (see Fig. 3).

Table 5 shows how the reduction of counts registered between 2 and 2.1 MeV in detectors of 2 and 4-kg is bigger for higher number of segments, combining longitudinal and transversal segmentation. For a 4-kg detector with the highest number of segments studied (66 segments distributed in 11 transversal slices and 6 angular sectors), approximately only 2 out of 100 events will not be rejected by anticoincidence techniques for  $^{60}\text{Co}$  contamination. For  $^{68}\text{Ge}$  the ratio is around 5 out of 100 events and for 2614.5 keV external gammas, less than a half of total events. This reduction can be observed qualitatively in the spectra obtained from simulations for the different background sources studied (see Fig. 4).

It is clear that for higher number of segments in the crystal, we are able to reject more background events. But the segmentation of a crystal is limited for some reasons. First

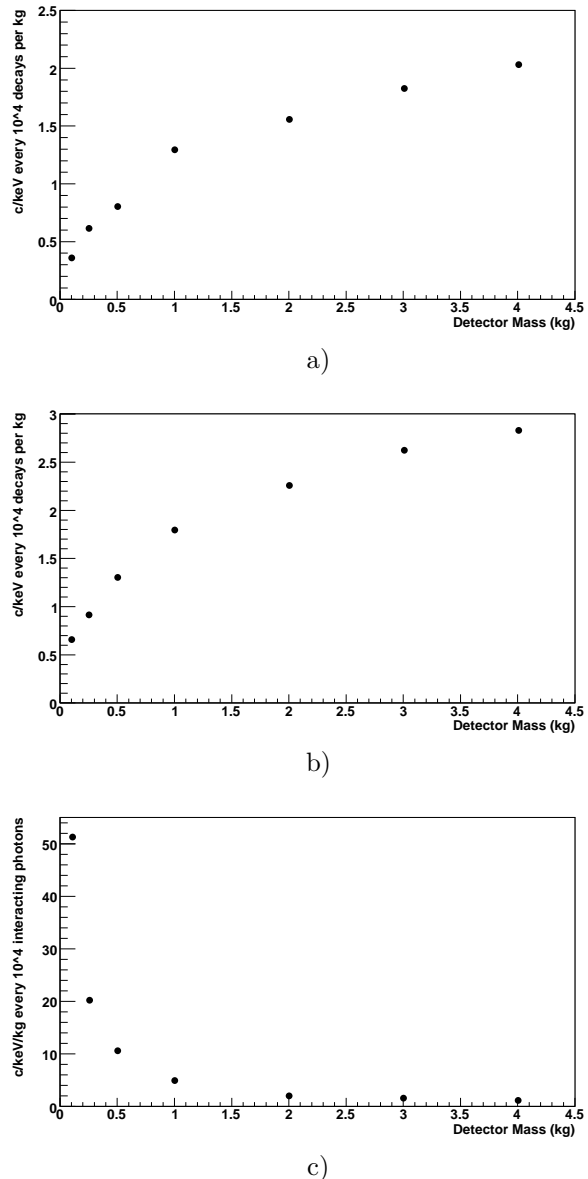


Fig. 2. Background level in the 2-2.1 MeV RoI depending on the component detector mass. For internal contaminations,  $^{60}\text{Co}$  (a) and  $^{68}\text{Ge}$  (b), it is represented in counts per keV every  $10^4$  decays per kg. For external photons of 2614.5 keV (c), it is represented in counts per keV per kg every  $10^4$  interacting photons.

of them is the difficulty associated to the reduction of the width of the transversal segments. It is also necessary to make a segmentation to reject a high number of background events without losing too much efficiency in the double beta decay events detection. The different segmentation configurations studied have transversal segments with a width of 1 cm approximately. This size is reachable using actual segmentation techniques and provides a good efficiency for the detection of double beta decay events, as it will be discussed later in Sec. 4.1.

Considering the biggest segmentation of all studied and applying the reduction factors obtained and shown in Table 5 to the raw rates for different background sources esti-

Table 5

Percentage of rejected events by crystal segmentation and anticoincidence techniques for registered events between 2 and 2.1 MeV. Different segmentation schemes for 2 and 4-kg detectors have been considered.

	2kg				4kg			
	7 planes		9 planes		9 planes		11 planes	
	&	&	&	&	&	&	&	
	7 planes	9 planes	6 sectors	6sectors	9 planes	11 planes	6 sectors	6 sectors
$^{60}\text{Co}$	92.4	95.6	97.0	98.2	94.9	96.7	97.6	98.4
$^{68}\text{Ge}$	86.1	90.7	93.2	95.1	89.8	92.7	94.2	95.7
external 2614.5 keV gammas	40.6	44.4	48.6	51.0	45.4	49.4	52.4	55.1

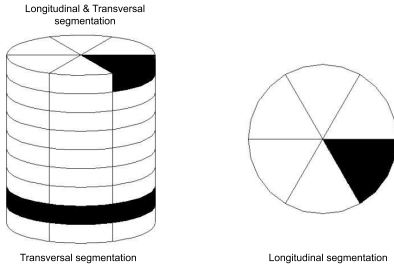


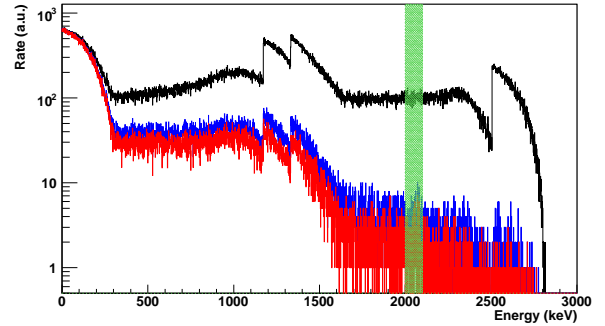
Fig. 3. Segmentation scheme for a germanium crystal with 9 transversal slices and 6 longitudinal sectors to obtain 54 segments.

mated in Sec. 2, the resulting rates can be derived and are presented in the first and third columns of Table 6.

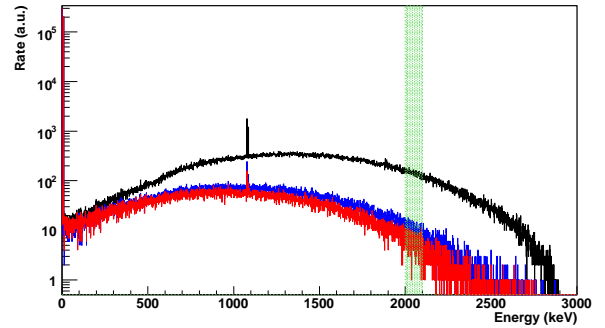
### 3.3. PSA

Besides the improvements made in the detector, like the segmentation of the crystal, a reduction of the background level from the analysis of the pulses registered can also be obtained. For this purpose, as pointed out before, it is necessary to distinguish between background and real double beta decay events in order to reject the first ones. Application of PSA in segmented crystals allows to increase the spatial resolution of conventional germanium detectors to obtain the position of energy deposits with a very good accuracy in all the dimensions [16] or at least a correct identification of the number of interaction points [40].

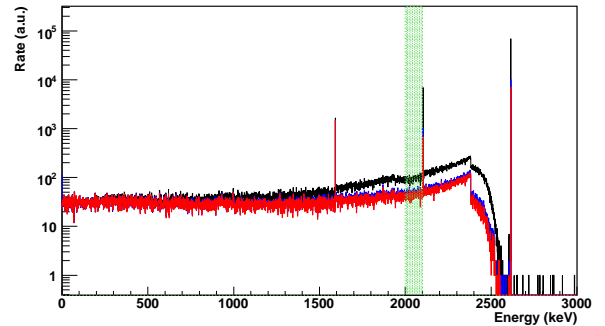
The data obtained in the simulations can be reanalyzed for a given spatial resolution, grouping all the partial energy deposits with a separation lower than the resolution and considering these groups like indivisible energy deposits. Then, it is possible to determine how many of these indivisible deposits each background event has. In figure 5, distributions of the number of energy deposits per event for different background sources and 4-kg detectors are showed, assuming 2 different values for the spatial resolution, 3 and 5 mm, which seem to be at reach today according to the



a)



b)



c)

Fig. 4. Comparison between the spectra obtained for the different contaminations studied:  $^{60}\text{Co}$  (a),  $^{68}\text{Ge}$  (b) and 2614.5 keV photons (c), for a 4-kg detector without segmentation (black line), with 11 transversal segments (blue line) and with 66 segments, 11 transversal by 6 longitudinal (red line).

Table 6

Estimates of counting rates (c keV<sup>-1</sup> kg<sup>-1</sup>y<sup>-1</sup>) in the 2-2.1 MeV RoI from cosmogenic contaminations and 2614.5 keV gamma emissions from <sup>208</sup>Tl in 2-kg and 4-kg germanium detectors, assuming maximum reduction factors deduced for segmented crystals using anticoincidence techniques and for segmented crystals using PSA. Same conditions for cosmogenic production and 2614.5 keV emissions than in Tables 3 and 4 are taken into account.

	2kg		4kg	
	segmentation	segmented PSA	segmentation	segmented PSA
<sup>60</sup> Co	5.2×10 <sup>-5</sup>	8.7×10 <sup>-6</sup>	6.0×10 <sup>-5</sup>	3.7×10 <sup>-6</sup>
<sup>68</sup> Ge	6.1×10 <sup>-4</sup>	1.4×10 <sup>-4</sup>	6.8×10 <sup>-4</sup>	1.3×10 <sup>-4</sup>
<sup>68</sup> Ge	1.5×10 <sup>-3</sup>	3.4×10 <sup>-4</sup>	1.7×10 <sup>-3</sup>	3.1×10 <sup>-4</sup>
external 2614.5 keV, 30 cm Pb	1.9×10 <sup>-2</sup>	1.8×10 <sup>-2</sup>	1.4×10 <sup>-2</sup>	1.3×10 <sup>-2</sup>
external 2614.5 keV, 40 cm Pb	1.8×10 <sup>-4</sup>	1.7×10 <sup>-4</sup>	1.4×10 <sup>-4</sup>	1.2×10 <sup>-4</sup>
intrinsic 2614.5 keV in lead	1.4×10 <sup>-3</sup>	1.2×10 <sup>-3</sup>	1.0×10 <sup>-3</sup>	8.9×10 <sup>-4</sup>
Best Total	2.2×10 <sup>-3</sup>	1.6×10 <sup>-3</sup>	1.9×10 <sup>-3</sup>	1.1×10 <sup>-3</sup>

work developed in Ref. [16]<sup>1</sup>; it is worth noting that these distributions have been obtained without making any particular definition of the segmentation scheme. The worst value of the spatial resolution can give an idea of the loss of rejection efficiency depending on the spatial resolution finally achieved. In Table 7, rejection factors after eliminating "multisite" events, between 2 and 2.1 MeV, are showed in function of the 2 values considered for the spatial resolution and for all background sources studied and 2 and 4-kg detectors. For the heaviest crystal and assuming a 3 mm spatial resolution, it is possible to reject 99.9% of background events coming from <sup>60</sup>Co, 99.2% from <sup>68</sup>Ge and 60.3% from 2614.5 keV photons; the values are 99.5%, 97.8% and 56.5% respectively if a resolution of 5 mm is considered.

Spatial resolution of the detectors allows to reject more or less background events depending on how the energy of these events is distributed in the crystal. One way to predict what could be the maximum reduction factor consists in determining the maximum distance between all the energy deposits of the same event (that we call maximum interdistance  $D_{max}$ , see Eq. 1) and studying how it is distributed.

$$D_{max} = \max[\sqrt{(x_i - x_j)^2 + (y_i - y_j)^2 + (z_i - z_j)^2}] \quad (1)$$

This maximum interdistance depends on different factors like the mass of the detector, the scheme of the decay of the isotope that produces the background event or the origin of the event, because it is different if the contamination is located inside the crystal or if comes from outside of the experimental setup. In Fig. 6, the distribution of these maximum interdistances for 2 and 4-kg detectors and all the background sources studied are presented, showing how all the factors mentioned previously have influence on these distributions. From these plots in Fig. 6, rejection factors

<sup>1</sup> A genetic algorithm for the decomposition of multiple hit events is presented in Ref. [16], considering the features of a cylindrical closed-end germanium detector with a mass of almost 2 kg and 6 angular sectors and 4 transversal slices. However, it is reported that the approach has no limitation concerning the geometry of the crystal, the number and layout of the segments or the number of interactions.

for any considered experimental spatial resolution can be deduced knowing that all events with a maximum interdistance lower than the spatial resolution will be labelled as "monosite" like double beta events.

Second and fourth columns in Table 6 show the expected counting rates in the 2-2.1 MeV RoI for background contributions in 2-kg and 4-kg germanium detectors, applying the reduction factors obtained when considering a 3D spatial resolution of 3 mm from PSA on the raw backgrounds estimates in Sec. 2. Total background levels have been calculated (see last row in Table 6) including cosmogenic <sup>60</sup>Co and <sup>68</sup>Ge in the detector as well as external and lead 2614.5 keV emissions and using the most favorable conditions, that is, adding values in first, second, fifth and sixth rows.

It must be noted that no technical limitation in the process of rejecting events thanks to coincidences between segments or PSA with a certain spatial resolution has been taken into account. Consequently, the rejection factors summarized in Tables 5 and 7 must be considered as the best ones achievable and give the limit of the power of these rejection techniques. Uncertainties in the total background levels presented in Table 6 must be dominated by the uncertainties in the raw backgrounds, discussed in Sec. 2, since statistical errors in the simulations are much smaller.

#### 4. Efficiency to neutrinoless DBD signal and sensitivity

The sensitivity of a neutrinoless DBD experiment is often evaluated using the detector factor-of-merit  $F_D$  defined as:

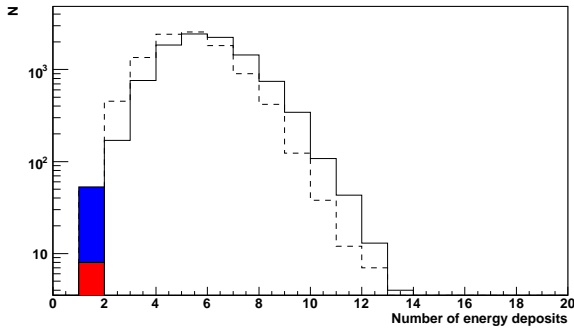
$$F_D = 4.17 \times 10^{26} \frac{f}{W} \sqrt{\frac{MT}{b\Delta E}} \epsilon \quad (2)$$

with  $f$  the isotopic abundance of the DBD emitter,  $W$  the atomic weight of the source material,  $MT$  the exposure of the experiment,  $b$  the background level (typically expressed in counts per keV, per kg and per y),  $\Delta E$  the energy window where the signal is expected to appear, dependant on the energy resolution of the detector, and  $\epsilon$  the detection efficiency.  $F_D$  is interpreted as the lifetime corresponding

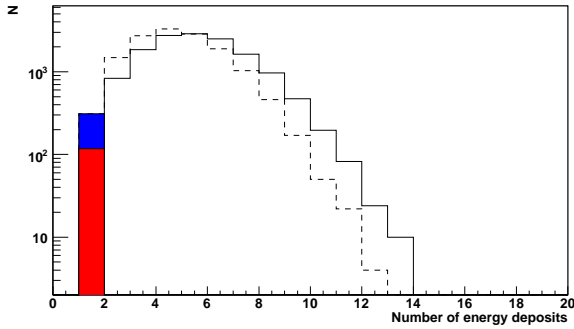
Table 7

Percentage of rejected events in the 2-2.1 MeV RoI by PSA techniques considering a spatial resolution of 3 and 5 mm for 2 and 4-kg detectors.

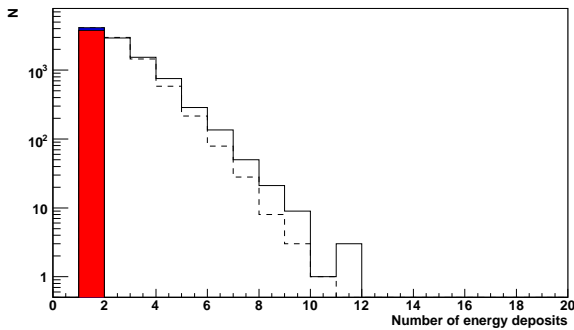
	2kg		4kg	
	3 mm	5 mm	3 mm	5 mm
	resolution	resolution	resolution	resolution
$^{60}\text{Co}$	99.7	99.0	99.9	99.5
$^{68}\text{Ge}$	98.9	97.0	99.2	97.8
external 2614.5 keV gammas	55.6	51.2	60.3	56.5



a)

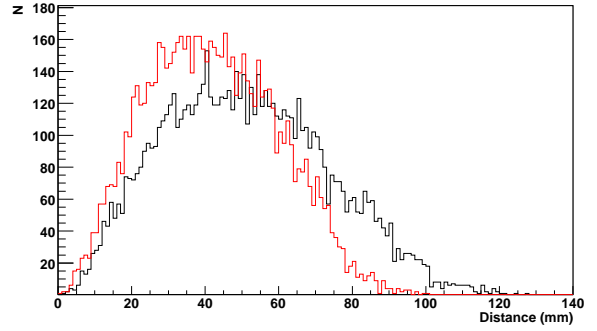


b)

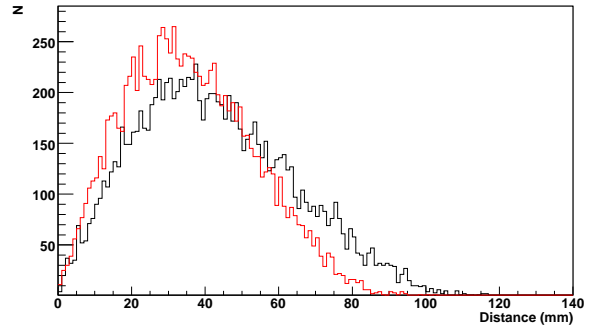


c)

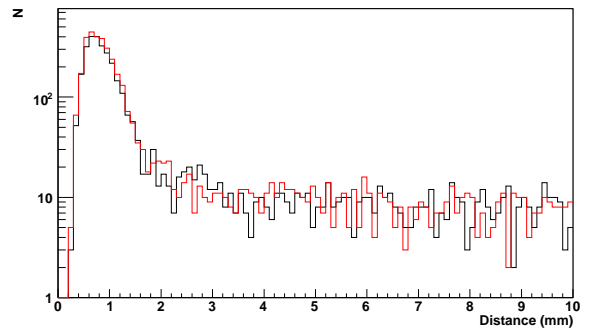
Fig. 5. Distribution of the number of energy deposits per event in the 2-2.1 MeV RoI for all the background contributions studied:  $^{60}\text{Co}$  (a),  $^{68}\text{Ge}$  (b) and 2614.5 keV photons (c), for 4-kg detector and considering a spatial resolution of 3 (solid line) and 5 mm (dashed line). Monosite events are singled out in red (blue) for 3 (5) mm resolution.



a)



b)



c)

Fig. 6. Distribution of the maximum interdistance between energy deposits of the same event in the 2-2.1 MeV RoI for  $^{60}\text{Co}$  (a) and  $^{68}\text{Ge}$  (b) internal contaminations and for 2614.5 keV external photons (c), for 2-kg (red line) and 4-kg (black line) detectors.

to the minimum detectable number of events over a background at  $1\sigma$  confidence level.

The neutrino effective masses which can be explored by an experiment with a detector factor-of-merit  $F_D$  can be

determined as:

$$\langle m_\nu \rangle^2 = \frac{m_e^2}{F_D F_N} \quad (3)$$

with  $m_e$  the electron mass and  $F_N$  the nuclear factor-of-merit, defined as  $F_N = G^{0\nu} |M^{0\nu}|^2$ , being  $G^{0\nu}$  a kinematical factor and  $M^{0\nu}$  the nuclear matrix element qualifying the likeliness of the transition.

The background level  $b$  achievable in germanium experiments has been analyzed in previous sections under different background reduction schemes; but the application of anticoincidence rejection or PSA techniques unfortunately affects also the efficiency for the detection of the neutrinoless DBD signal. Therefore, a study of this efficiency has been carried out and is presented here.

#### 4.1. Efficiency to signal

In order to evaluate the dependency between background reduction techniques and loss of efficiency, it is necessary to simulate neutrinoless DBD ( $0\nu\beta\beta$ ) events inside the detector to apply them the same treatment that a background event. This procedure allows to estimate the percentage of  $0\nu\beta\beta$  events rejected losing detection efficiency. Signal events can be missed either because of the escape of the Bremsstrahlung radiation produced by electrons or because  $0\nu\beta\beta$  events are mistaken as background due to the spatial distribution of their energy deposits.

To define  $0\nu\beta\beta$  events in the simulations, two electrons with sum energy of 2040 keV (Q value for  $^{76}\text{Ge}$  DBD) have been considered, neglecting in first approach the angular correlation between electrons. In order to check if this angular correlation could have substantial influence to detect a  $0\nu\beta\beta$  event, a first study was made simulating two electrons of 1020 keV each emitted randomly, with the same and with opposite directions. Decays are distributed homogeneously in the crystals, for 2 and 4-kg detectors. Tables 8 and 9 show that the differences between the detection efficiency factors in the cases described before are less than 1% for the different angular correlations considered, validating the approximation taken.

Another point in the simulation of  $0\nu\beta\beta$  events is the energy distribution of the two electrons. Four different configurations were studied: two electrons of 1020 keV each (half of the total energy), two electrons of 1500 and 540 keV, two electrons of 1734 and 306 keV (75% and 25% of the full energy respectively) and one electron of 2040 keV. It is important to point that the last case is not a real case but could be useful to obtain limit values in the detection efficiency because Bremsstrahlung probability is higher for more energetic electrons. For all these energy configurations, the electrons were emitted in random directions using the same simulation package that for the background events. Figure 7 shows an example of the spectrum registered in the detector after the simulation of  $0\nu\beta\beta$  events. In this case in particular, two electrons of 1020 keV each were emitted in

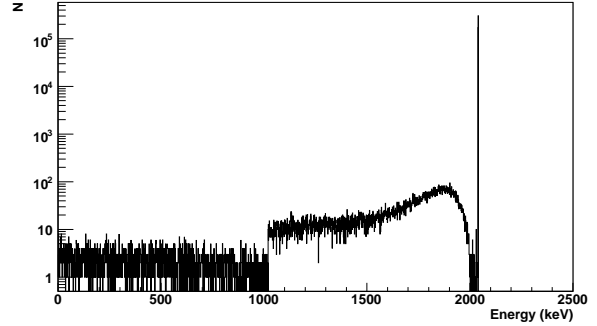


Fig. 7. Energy spectrum registered for simulated  $0\nu\beta\beta$  events composed by 2 electrons of 1020 keV each emitted in random directions in a 4-kg detector.

a 4-kg detector. Three different regions can be identified in this spectrum:

- Up to 1020 keV, energy is lost from both electrons, either by escape of Bremsstrahlung radiation and/or escape of the electron itself (if the decay is close enough to the detector surface). The probability that this happens for both electrons is quite low and for this reason a step appears at 1020 keV.
- From 1020 keV up to the peak, events where one electron deposits all the energy and the other one suffers Bremsstrahlung losses or escapes from the detector, are registered. In a smaller percentage, events where both electrons do not deposit the full energy can appear here too.
- In the peak, electrons have deposited the full energy. This is the region where the  $0\nu\beta\beta$  signal is expected. As explained later, some events in the peak can be labelled as "multisite" events and therefore rejected as background, when electrons produce Bremsstrahlung emission which is finally absorbed in the crystal.

Using the simulation of  $0\nu\beta\beta$  events, the relationship between the detection efficiency and the detector mass, directly related with the granularity of a future experiment, can be analyzed. Tables 8 and 9 show, for two 1020 keV electrons, that the difference between the detection efficiency for 2 and 4-kg detectors is less than 1% for all the background rejection configurations, but always better for the heaviest detector. For this reason, the studies of the different energy configurations were made for a 4-kg crystal.

Table 10 summarizes the detection efficiencies obtained in a 4-kg detector for the different energy configurations in  $0\nu\beta\beta$  events. Two main conclusions can be obtained from this table. One is that PSA techniques offer better detection efficiency than background rejection based just on crystal segmentation. The explanation is that the anticoincidence between segments rejects all the  $0\nu\beta\beta$  events with energy deposits in two or more segments of the crystal, while PSA rejects events with two separated energy deposits, typically due to Bremsstrahlung but, in principle, could allow events close to the borders. A useful information to understand this is the maximum distance between all the energy

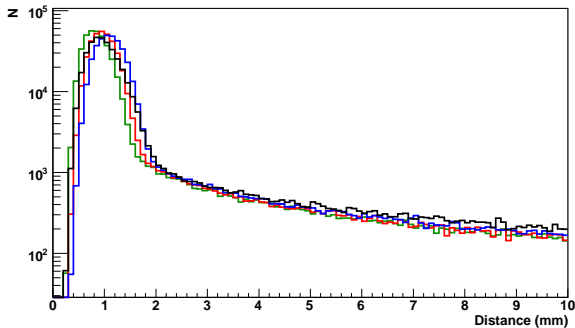


Fig. 8. Distribution of the maximum interdistance between energy deposits of the same  $0\nu\beta\beta$  event at the peak in a 4-kg detector for 2 electrons of 1020 keV each (green), 1500 + 540 keV electrons (red), 1734 + 306 keV electrons (blue) and one 2040 keV electron (black).

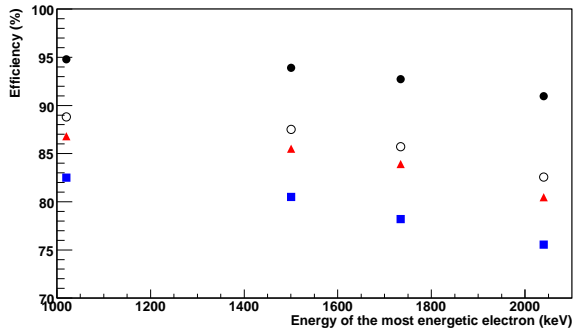


Fig. 9. Detection efficiency versus the energy of the most energetic electron of a  $0\nu\beta\beta$  event in a 4-kg detector considering a full crystal detector (black points), anticoincidences in 11 x 6 segmented crystals (blue squares), and PSA with 3 mm (red triangles) and 5 mm (white circles) spatial resolution.

deposits obtained in the simulation for  $0\nu\beta\beta$  events (the maximum interdistance defined in Section 3.3 and calculated using Eq. 1). Figure 8 shows the distribution of the interdistances for signal events and for all the energy configurations studied in a 4-kg detector. In all the cases, most of the events have a maximum interdistance below 3 mm, ensuring that they will be considered as "monosite" events by PSA and can be separated safely from background ones.

The other important point from Table 10 is the dependency between the efficiency and the energy of the most energetic electron of the  $0\nu\beta\beta$  event. The more equal the electron energies, the higher the detection efficiency. This relationship is logical due to the Bremsstrahlung probability, that grows proportional to the energy of the electron. For this reason, the non real case of a 2040 keV electron can be useful to estimate the lower limit of the detection efficiency. The obtained dependencies of the detection efficiency on electron energy can be fitted to a grade two polynomial, for the different background rejection configurations considered (as shown in Fig.9); convoluting this polynomials with the single electron spectrum of  $0\nu\beta\beta$  decays in  $^{76}\text{Ge}$ , an overall value for the efficiency to signal can be estimated. Last row in Table 10 presents these results.

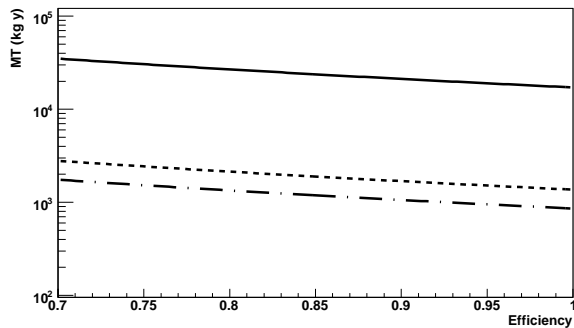


Fig. 10. Exposure MT (in kg-y) necessary to reach the sensitivity to explore neutrino effective masses  $\langle m_\nu \rangle > 40$  meV, versus the detection efficiency to  $0\nu\beta\beta$  events considering full crystals (solid line), anticoincidences in 11 x 6 segmented crystals (dashed line), and PSA with a spatial resolution for PSA of 3 mm (dot and dash line).

## 4.2. Sensitivity

The overall detection efficiency to signal estimated above has been used together with Eqs. 2 and 3 to compare the sensitivity of germanium DBD experiments using different background rejection schemes. Three different situations have been taken into consideration: no rejection technique, the application of anticoincidence rejection for crystals with  $6 \times 11$  segments, and the use of PSA techniques assuming a 3 mm spatial resolution. Detectors enriched in  $^{76}\text{Ge}$  at 86% and total exposures of  $\text{MT}=100$  and  $1000$  kg-y have been assumed. An energy window of 3.5 keV has been considered, as in Ref. [3]. Values of background level and corresponding detection efficiency deduced in this work for 4-kg crystals have been used for each situation. Table 11 summarizes the evaluated sensitivities, presenting the  $F_D$  values and the corresponding effective neutrino masses considering the average nuclear factor-of-merit  $F_N=7.3 \times 10^{-14} \text{ y}^{-1}$  used in Ref. [3]. Neutrino masses below 50 meV can be explored with very segmented crystals or applying PSA techniques and for high enough exposures.

To achieve a certain sensitivity to the effective neutrino mass, the required exposure of an experiment depends on the background level in the region of interest and the detection efficiency to the signal (see Eqs. 2 and 3); both background level and efficiency are different when different background rejection schemes are considered. Figure 10 shows this dependency between the exposure and the efficiency in the three background rejection schemes considered before. Using the overall signal efficiency values previously estimated, it can be deduced from this plot that despite the loss of efficiency, segmented crystals working in anticoincidence require an exposure one order of magnitude lower than that of non segmented detectors to explore the same range of neutrino masses. If PSA techniques are used with 3 mm of energy resolution, an additional factor of  $\sim$ two of reduction is achieved in the necessary exposure.

Table 8

Detection efficiency (%) for  $0\nu\beta\beta$  events composed by two electrons of 1020 keV each emitted in random, opposite and same directions. Different background rejection configurations are considered, for 2-kg detectors.

		segmentation				PSA	
		7 planes 9 planes		7 planes 9 planes		3 mm 5 mm	
	full crystal	7 planes	9 planes	6 sectors	6 sectors	3 mm	5 mm
random direction	93.6	86.1	84.3	82.9	81.3	86.4	88.3
same direction	93.8	86.7	84.9	83.8	82.1	86.6	88.5
opposite direction	93.6	85.7	83.8	82.3	80.5	86.4	88.2

Table 9

As table 8, but for 4-kg detectors.

		segmentation				PSA	
		9 planes 11 planes		9 planes 11 planes		3 mm 5 mm	
	full crystal	9 planes	11 planes	6 sectors	6 sectors	3 mm	5 mm
random direction	94.7	86.4	84.8	83.7	82.4	86.8	88.7
same direction	94.8	86.9	85.5	84.5	83.2	87.0	88.8
opposite direction	94.6	85.9	84.3	83.1	81.7	86.9	88.7

Table 10

Detection efficiency (%) for  $0\nu\beta\beta$  events composed by two electrons emitted in random directions with different energy schemes. Different background rejection configurations are considered for 4-kg detectors. Last row shows an overall efficiency taking into account the single electron  $0\nu\beta\beta$  spectrum.

		segmentation				PSA	
		9 planes 11 planes		9 planes 11 planes		3 mm 5 mm	
	full crystal	9 planes	11 planes	6 sectors	6 sectors	3 mm	5 mm
2 x 1020 keV	94.7	86.4	84.8	83.7	82.4	86.8	88.7
1500 + 540 keV	93.9	84.8	83.1	82.0	80.5	85.6	87.5
1734 + 306 keV	92.9	82.9	81.0	79.8	78.2	83.9	85.8
2040 keV	90.9	80.1	78.3	77.0	75.5	80.4	82.5
single electron	93.8	84.6	82.9	81.7	80.3	85.4	87.3
$0\nu\beta\beta$ spectrum							

Table 11

Comparison of the sensitivity of germanium DBD experiments under different background rejection schemes, evaluated following Eqs. (2) and (3) (see text).

	MT (kg·y)	b (c keV <sup>-1</sup> kg <sup>-1</sup> y <sup>-1</sup> )	$\epsilon$ (%)	$F_D$ (10 <sup>26</sup> y)	$\langle m_\nu \rangle$ (meV)
no rejection	100	0.022	93.8	1.6	149
6×11 segmentation	100	0.0019	80.3	4.7	88
PSA (3 mm resolution)	100	0.0011	85.4	6.5	74
no rejection	1000	0.022	93.8	5.1	84
6×11 segmentation	1000	0.0019	80.3	15	49
PSA (3 mm resolution)	1000	0.0011	85.4	21	42

## 5. Discussion and conclusions

Some conclusions can be drawn from the analysis of the different strategies for background reduction in germanium double beta decay experiments. The study of the granularity of the detector system shows that heavier crystals are better to reduce the contribution of external radioimpurities, but worse to reduce background coming from internal contaminations. By applying the most powerful segmentation techniques taken here into consideration in a 4-kg detector, 2(5) out of 100 events due to internal impurities from  $^{60}\text{Co}$  ( $^{68}\text{Ge}$ ) would remain in the RoI, while for external contaminations, about half of the events would be rejected. A 3-dimensional spatial resolution of 3 mm, obtained by means of PSA in segmented detectors, would allow to reject more than 99% of background events due to cosmogenic isotopes induced in the crystal, and around 60% of those coming from external 2614.5 keV photons.

According to numbers presented in Table 6, a background level of  $1.1$  ( $1.6$ )  $10^{-3}$   $\text{c keV}^{-1} \text{kg}^{-1}\text{y}^{-1}$  due to the studied background sources could be achieved using 4 (2)-kg crystals when considering very precise conditions. For the production of  $^{60}\text{Co}$  ( $^{68}\text{Ge}$ ), the exposure time is of 30 (180) days and the production rate is 5 (1)  $\text{kg}^{-1}\text{d}^{-1}$ . In the case of  $^{68}\text{Ge}$ , a cooling time of 180 days has been also taken into account. For the external 2614.5 keV, an environmental flux of  $0.1 \text{ cm}^{-2} \text{ s}^{-1}$  has been assumed and the use of a 40-cm-thick lead shield considered. For intrinsic  $^{232}\text{Th}$  impurities in the lead shielding, the activity supposed is  $1 \mu\text{Bq/kg}$ . In these optimal conditions, the raw background is reduced by more than one order of magnitude thanks to a 3 mm spatial resolution achieved by PSA in segmented detectors. The most relevant contribution is that of the 2614.5 keV produced in the lead shielding itself by  $^{232}\text{Th}$  impurities, followed by the one from cosmogenic  $^{68}\text{Ge}$  induced in the crystal. External 2614.5 keV photons and cosmogenic  $^{60}\text{Co}$  are almost negligible. The use of large crystals, having less background for external contaminations than the small ones, seems more adequate since background rejection by anticoincidence between segments or by PSA is efficient enough in the reduction of contributions from internal radioimpurities.

Some comments are in order if considering other less favorable conditions for the raw background or the rejection strategies:

- Contribution from  $^{60}\text{Co}$  emissions is in general negligible thanks to the very good rejection factors attainable either with PSA in segmented detectors or just anticoincidence techniques between segments of the detectors.
- $^{68}\text{Ge}$  contribution in the scenario described above considering a production rate of  $1 \text{ kg}^{-1}\text{y}^{-1}$  is very small. However, it must be noticed that the production rate calculated in different estimates presented in Sec. 2.1.1 is much higher. It has been shown that if the production rate was 10 times bigger, a cooling time of 2 years instead of 3 months would be necessary to achieve background

contributions of the same order of magnitude.

- To shield external 2614.5 keV photons from environmental gamma radiation in the laboratory, 40 cm of lead are mandatory. When using just 30 cm, the goal of a background level of  $10^{-3} \text{ c keV}^{-1} \text{kg}^{-1}\text{y}^{-1}$  cannot be fulfilled.
- Regarding intrinsic  $^{232}\text{Th}$  impurities in the lead shield, it is worth noting that the achievement of a radiopurity of  $1 \mu\text{Bq/kg}$  cannot be taken for granted since common upper limits to contaminations of this chain achieved in lead are of some hundreds of  $\mu\text{Bq/kg}$  (see for instance the ILIAS database on radiopurity measurements<sup>2</sup> and even the best limits obtained with the most modern germanium spectrometers are of some tens of  $\mu\text{Bq/kg}$  [38,39]. Therefore, to further reduce the background level from this source, improvement of the radiopurity of this material or using radiopure copper instead of lead in the inner part of the shielding would be very useful. It has also been proved that increasing the thickness of the lead layer is not relevant for these shielding radioimpurities.
- For the spatial resolution, if a worse performance of 5 mm was achieved, the best total background level would be of  $1.5$  ( $2.0$ )  $10^{-3}$   $\text{c keV}^{-1} \text{kg}^{-1}\text{d}^{-1}$  for 4 (2)-kg crystals. No dramatic difference in the background level from 2614.5 keV would be produced, while an increase in a factor of  $\sim 3$  (4) would be registered for  $^{68}\text{Ge}$  ( $^{60}\text{Co}$ ) emissions, which, fortunately, seem not to be the dominant background source.
- The use of 4-kg crystals gives a more reduced background, but 2-kg detectors, in use for a long time, could be acceptable. Segmentation schemes assumed are feasible for present germanium detector technologies and give a best total background level of  $1.9$  ( $2.2$ )  $10^{-3}$   $\text{c keV}^{-1} \text{kg}^{-1}\text{y}^{-1}$  for 4 (2)-kg crystals. Therefore, the option of applying just segmentation techniques must not be discarded.

The overall detection efficiency to neutrinoless DBD signals has been evaluated by Monte Carlo simulation for the different background rejection scenarios, finding for 4-kg crystals a reduction from  $\sim 94\%$  to  $\sim 80\%$  when considering anticoincidences in  $11 \times 6$  segments and to  $\sim 85\%$  if PSA techniques are applied with a 3 mm spatial resolution.

The sensitivity of DBD experiments depends on both achieved background level in the RoI and detection efficiency; it has been shown that the improvement in the former thanks to rejection techniques largely compensates the loss in the latter since experiments with these techniques require much lower exposure for a fixed sensitivity.

In summary, it seems that contribution from dominant background sources in previous germanium double beta decay experiments could be reduced down to  $10^{-3} \text{ c keV}^{-1} \text{kg}^{-1}\text{y}^{-1}$  in the RoI using present detector technologies, which allows to explore effective neutrino masses even below 50 meV.

<sup>2</sup> Available at <http://radiopurity.in2p3.fr/>. and developed within the ILIAS (Integrated Large Infrastructures for Astroparticle Science) EU project.

## 6. Acknowledgments

This work has been funded by Spanish MEC contract FPA2004-0974 and the ILIAS (“Integrated Large Infrastructures for Astroparticle Science”) EU project (contract number: EU-RII3-CT2003-506222). Useful discussions within the IDEA (“Integrated Double-beta decay European Activities”) Joint Research Activity 2 in ILIAS are deeply acknowledged.

## References

- [1] S. R. Elliot and P. Vogel, *Ann. Rev. Nucl. Part. Sci.* 52 (2002) 115-151; S.R. Elliott and J. Engel, *J.Phys. G*30 (2004) R183; A. Piepke, *Nucl. Phys. A* 752 (2005) 42-52.
- [2] A. Morales, *Nucl. Phys. B (Proc. Suppl.)* 77 (1999) 335-345
- [3] F. T. Avignone III, G. S. King III and Yu G. Zdesenko, *New Journal of Physics* 7 (2005) 6.
- [4] G. Douysset et al., *Phys. Rev. Lett.* 86 (2001) 4259.
- [5] L. Baudis et al., *Phys. Rev. Lett.* 83 (1999) 41.
- [6] C. E. Aalseth et al., *Phys. Rev. D* 65 (2002) 092007.
- [7] The Majorana Collaboration, “White Paper on the Majorana Zero-Neutrino Double-Beta Decay Experiment”, [arXiv:nucl-ex/0311013].
- [8] I. Abt et al., GERDA Letter of Intent, “A new  $^{76}\text{Ge}$  Double Beta Decay Experiment at LNGS”, [arXiv:hep-ex/0404039].
- [9] P. Sangsingkeow et al., *Nucl. Instr. and Meth. A* 505 (2003) 183-186.
- [10] Th. Kröll and D. Bazzacco, *Nucl. Instr. and Meth. A* 463 (2001) 227-249.
- [11] S. R. Elliot et al., *Nucl. Instr. and Meth. A* 558 (2006) 504-510.
- [12] I. Abt et al., submitted to *Nucl. Instr. and Meth. A*, [arXiv:nucl-ex/0701004]. I. Abt et al., submitted to *Nucl. Instr. and Meth. A*, [arXiv:nucl-ex/0701005].
- [13] T. Niedermayr et al., *Nucl. Instr. and Meth. A* 553 (2005) 501-511.
- [14] M. Descovich et al., *Nucl. Instr. and Meth. A* 553 (2005) 512-521; M. Descovich et al., *ibid.*, 535-542.
- [15] C. E. Svensson et al., *Nucl. Instr. and Meth. A* 540 (2005) 348-360.
- [16] Th. Kröll and D. Bazzacco, *Nucl. Instr. and Meth. A* 565 (2006) 691-703.
- [17] D. González et al., *Nucl. Instr. and Meth. A* 515 (2003) 634-643.
- [18] G. Heusser, *Annu. Rev. Nucl. Part. Sci.* 45 (1995) 543.
- [19] J. A. Formaggio and C. J. Martoff, *Annu. Rev. Nucl. Part. Sci.* 54 (2004) 361.
- [20] C. E. Aalseth et al., *Phys. Rev. C* 59 (1999) 2108.
- [21] I. Abt et al., *Nucl. Instr. and Meth. A* 570 (2007) 479-486.
- [22] L. Pandola et al., *Nucl. Instr. and Meth. A* 570 (2007) 149-158.
- [23] S. Agostinelli et al, *Nucl. Instr. Meth. A* 506 (2003) 250. Web page: <http://www.cern.ch/geant4>.
- [24] S. Cebrián et al., *Journal of Physics: Conference Series* 39 (2006) 344-346, Institute of Physics.
- [25] Horiguchi T et al. 1983 *Int. J. Appl. Rad. Isot.* 34 1531-5
- [26] Aleksandrov Y V et al. 1995 *Bull. Russian Acad. Sci. - Phys. Ser.* 59 895
- [27] Norman E B et al. 2005 *Nucl. Phys. B (Proc. Suppl.)* 143 508
- [28] Silberberg R et al. 1998 *Astrophys. J.* 501911-
- [29] Shubin Y N et al. 1995 Cross-section data library MENDL-2 to study activation as transmutation of materials irradiated by nucleons of intermediate energies, report INDC(CCP)-385 (IAEA)
- [30] Van Riper K A et al. 2001 *Nucl. Instr. Meth. A* 463 576-85, LA-UR-99-360.
- [31] Koning A J et al. 1998 Neutron and Proton Transmutation-Activation Cross Section Libraries to 150 MeV for Application in Accelerator-Driven Systems and Radioactive Ion Beam Target-Design Studies, ECN Report ECN-R-98-012 (Petten, The Netherlands). Chadwick M B et al. 1999 LA150 Documentation of Cross Sections, Heating, and Damage LA-UR-99-1222.
- [32] Ziegler J F 1998 *IBM J. R&D* 42 117-40
- [33] L. Baudis et al., *Nucl. Instr. Meth. A* 481 (2002) 149
- [34] Miley H et al. 1992 *Nucl. Phys. B (Proc. Suppl.)* 28A 212-5
- [35] Avignone F T et al. 1992 *Nucl. Phys. B (Proc. Suppl.)* 28A 280-5
- [36] E. Bellotti et al., *Journal of Physics: Conference Series* 39 (2006) 338-340, Institute of Physics.
- [37] G. Luzón et al., to appear in *Proc. of the 6th International Workshop on the Identification of Dark Matter (IDM2006)*, Rhodes (Greece), 11th-16th September 2006.
- [38] G. Heusser et al., *Proceedings of the Topical Workshop on Low Radioactivity Techniques 2004*, Sudbury (Canada), American Institute of Physics Conference Proceedings 785 (2005) p. 39-47.
- [39] M. Laubenstein et al., *Appl. Radiation and Isotopes* 61 (2004) 167-172.
- [40] F. C. L. Crespi, *Nucl. Instr. and Meth. A* 570 (2007) 459-466.